Chapter 5

Anatomy of the mean and seasonal Leeuwin Current

5.1 INTRODUCTION

The Lagrangian particles in the previous chapter suggest complex circulation linked with the Leeuwin Current and water mass transformation processes. Herein we generate a quantitative picture of the structure, volume transport and transport–weighted properties of the mean and seasonal Leeuwin Current off the west Australian coast between 22°S and 34°S, using the 5–year long POP11B outputs, from 1993 to 1997 [model details in **Appendix C**]. This will lay the foundation for understanding of the heat budget of the Leeuwin Current in **Chapter 6**.

5.2 METHOD

The 5–year averaged Leeuwin Current along the west Australian coast is defined using a "mask" based on its three dimensional structure. By averaging along longitude and/or depth views of the Leeuwin Current reveal its varying properties. The offshore limit of the mask was set according to a threshold on the magnitude of the cross–shore gradient of sea surface height (SSH) that clearly followed the outer edge of the Leeuwin Current (not shown). All the mean poleward flow between the offshore limit of the mask and the coast was automatically assigned as "Leeuwin" but, for improved precision, we have also manually refined the mask. This improved mask does capture the bulk of the Leeuwin Current but may leave out some part of it that was not clearly distinguishable from the adjacent ocean. The vertical sections (0–800 m depth) also include any flow below the Leeuwin Current, such as the bulk of the equatorward–flowing Leeuwin Undercurrent along the upper slope and a small part of a weak poleward flow below it. None of the velocity components has been rotated into principal angles of variance, though the magnitude as well as the spatial pattern of the meridional velocity are nearly equivalent to the absolute velocity (**V**, not shown).

5.3 MEAN

5.3.1 Current structure and property distributions

An overview of the 5–year mean Leeuwin Current in the context of the southeast Indian Ocean is illustrated by a model slice taken at its core depth in **Figure 5.1**. The Leeuwin Current appears as an eastern boundary jet – flowing more strongly between the shelf break (~200 m) and the continental slope (~1000 m) – which transports relatively fresher and warmer Tropical Water poleward. Although the fastest poleward velocities are observed offshore of the 200 m isobath, the freshest and warmest water is seen just inshore of that isobath, at least in latitudes lower than 30°S. The near surface width of the Leeuwin Current varies from ~80 to 145 km. It progressively deepens from 150 m at 22°S to 300 m at 34°S [**Figure 5.2**, top panel]. Below the Leeuwin Current lies the equatorward flow of the Leeuwin Undercurrent and, below the undercurrent, a weak poleward flow.

The Leeuwin Current has maxima at three surface sites along the coast exactly where the cross–shore SSH gradients are largest (tighter contours), being greater than –18 cm s^{-1} near 26°–27°S and 28°–29°S, and greater than –20 cm s^{-1} south of 33°S [**Figure 5.1**]. Poleward flow does not uniformly accelerate downstream but is fastest near 34°S [**Figure 5.2**, top panel]. The equatorward maxima of the Leeuwin Undercurrent (3 cm s^{-1}, 2 cm s^{-1} and 7 cm s^{-1}) lie at same latitude bands, also being fastest near 34°S but by more than double of the other two maxima. The zonal velocity [**Figure 5.2**, middle panel] predominantly reflects the alignment of the coastline [**Figure 5.1**] and its maxima are closely associated with the sites of the meridional ones. Weak upwelling ($\leq 10^{-3}$ cm s^{-1}) is observed in the upper portion (top 50–100 m) of the Leeuwin Current whereas the lower portion comprises downwelling [**Figure 5.2**, bottom panel]. Downwelling also occurs over most of the Leeuwin Undercurrent, and only its deepest portion shows upwelling.

The properties of the water advected by the Leeuwin Current gradually changes from more tropical (fresher, warmer, lighter) at lower latitudes to more subtropical (saltier, cooler, denser) at higher latitudes [**Figure 5.2**]. The salinity distribution displays a subsurface minimum of 34.9–35 psu at 50 m depth north of 26°S, and maxima (≥ 35.5 psu) at the deepest part of the Leeuwin Current (and upper part of the Leeuwin Undercurrent) between 26°–31°S and over its entire depth south of 33°S [top panel]. The θ and σ_θ distributions are very similar, and both slope upward in the downstream direction within the Leeuwin Current due to continuous cooling and increasing salinity [middle and bottom panels]. Towards higher latitudes, the thickness of isopycnal layers is broader and hence the stratification of the Leeuwin Current becomes weaker, suggesting a strong role for surface cooling in current properties. This transformation by air–sea fluxes results in cross isopycnal flow in the mixed layer. However, lateral exchanges (inflows and outflows) must also be important, such as in the case of the deep

salinity maximum clearly observed in the Leeuwin Current and undercurrent between 26°–31°S, which is linked with open ocean near surface eastward jets that downwell to ~200 m and join the boundary flow [see **Chapter 4**].

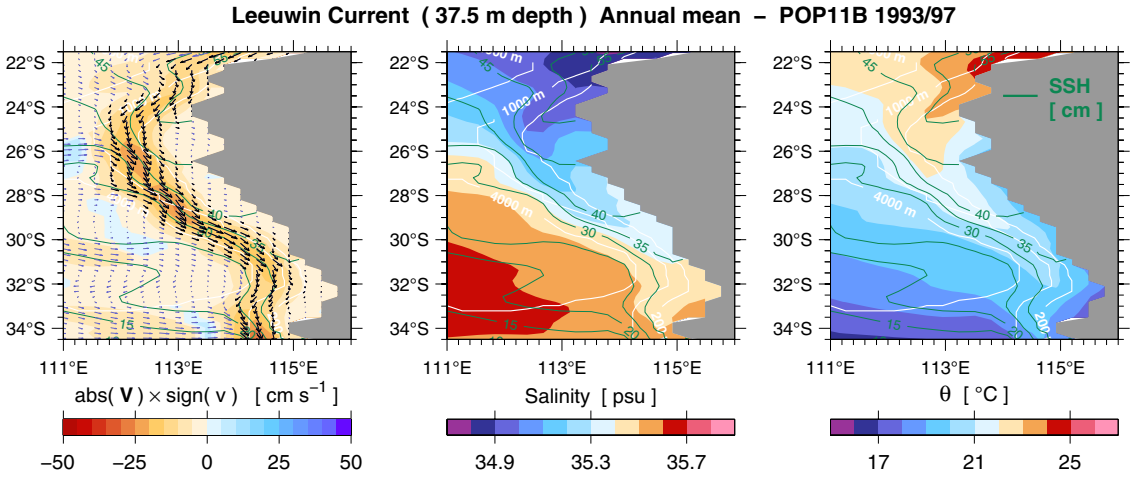

Figure 5.1. Mean horizontal maps at 37.5 m depth. Velocity vectors (left), salinity (middle) and θ (right). Velocity vectors are superimposed on the absolute speed (**V**) multiplied by the sign of the meridional velocity (+N). SSH contours are indicated in green and isobaths in white. Vectors in black are part of the "mask" (see text).

5.3.2 Volume transport and transport–weighted properties

The volume transport of the mean Leeuwin Current [**Figure 5.3**, top panel] was calculated by integrating the product of the meridional velocity and its grid cell area over longitude and depth, for each latitude grid point in the model between 22° and 34°S which was part of the Leeuwin Current's mask [**Section 5.2**]. The heat, salt and density fluxes are presented in terms of transport–weighted properties (hereafter TW θ, TW S and TW σ_θ respectively). The estimates were calculated by integrating the product of the property in question and the meridional velocity over their grid cell area, in longitude and depth, and then dividing by the total volume transport:

$$\text{TW } \phi = \frac{\iint \phi v dx dz}{\int v dx dz} \qquad \text{[Equation 5.1]}$$

where:

ϕ is property

v is meridional velocity

dx is the grid cell horizontal distance (longitude)

dz is the grid cell vertical distance (depth).

The magnitude of the poleward transport of the Leeuwin Current off Western Australia can be divided into three regimes:

(i) 22°–27°S, steeply increasing from –1.2 to –2.3 Sv (gains –1.1 Sv);

(ii) 27°–33°S, gently decreasing to a minimum of –1.5 Sv (loses –0.8 Sv);

(iii) 33°–34°S, abruptly increasing over a short distance to –2.2 Sv (gains 0.7 Sv).

The values above depend on the magnitude of the meridional velocity and the size of the area. Basically where the poleward velocity increases in (i) and (iii), the areas decrease, being the opposite valid for the (ii) regime [**Figure 5.3**, top panel]. The velocity curve in the top panel closely follows the cross–shore gradient of SSH shown in the middle panel, even though this gradient was simply taken along the jet axis position (current maximum). This confirms that the poleward flow of the Leeuwin Current is predominantly in geostrophic balance, as initially hinted by the comparison of the velocity field at 37.5 m depth and the SSH pattern in **Figure 5.1**. Its jet axis is found on the shelf/slope over the 200–700 m isobaths. By plotting the bottom depth below the jet axis we find that the jet moves deeper when the current is broadest and slower in the (ii) regime. Overall, when the Leeuwin decelerates, it becomes wider and its axis moves farther offshore, and vice–versa for when it accelerates. Assuming that the net vertical velocity at the bottom of the Leeuwin Current and the net inshore cross–shelf exchange (shelf is not well resolved by the grid resolution of the model) are both small, the variations in the magnitude of the poleward transport in each of those three regimes must be explained by lateral exchanges (net inflows and outflows) along the outer edge of the current. In **Chapter 4**, under a Lagrangian framework, we have shown that at the same time the Leeuwin Current is augmented by zonal eastward jets, it can transfer part of its transport to the offshore ocean through temporary westward diversions of the boundary flow (e.g., offshoots and filaments) and shedding of mesoscale eddies.

The linear drop in SSH [**Figure 5.3**, middle panel] over the axis of the Leeuwin Current is explained by the current starting light at 22°S and ending up denser at 34°S [bottom panel]. The transport–weighted properties in the bottom panel show that along its path, between 22°S and 34°S, the depth–averaged Leeuwin Current cools by ~6°C, becomes saltier by ~0.6 psu, and thus denser by ~2 kg m^{-3}. Since these trends are practically linear with latitude they may indicate that there are no hot spots for changes in the water properties carried by the Leeuwin Current.

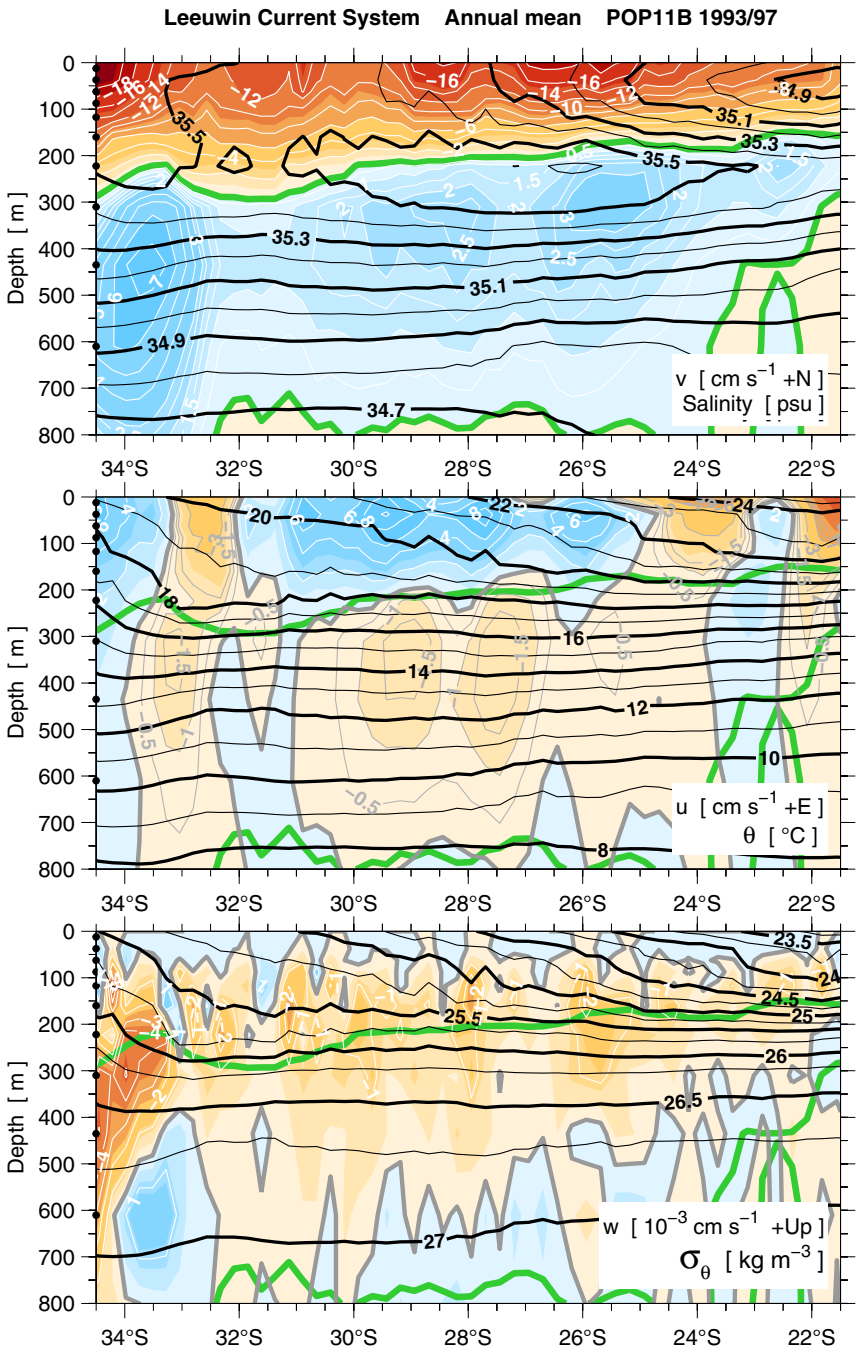

Figure 5.2. Vertical sections of the zonally–averaged mean Leeuwin Current. Salinity and meridional velocity (top). θ and zonal velocity (middle). σ_θ and vertical velocity (bottom). The bold green contour is the meridional velocity zero line on all plates. Note that these properties are volume averaged and not transported averaged.

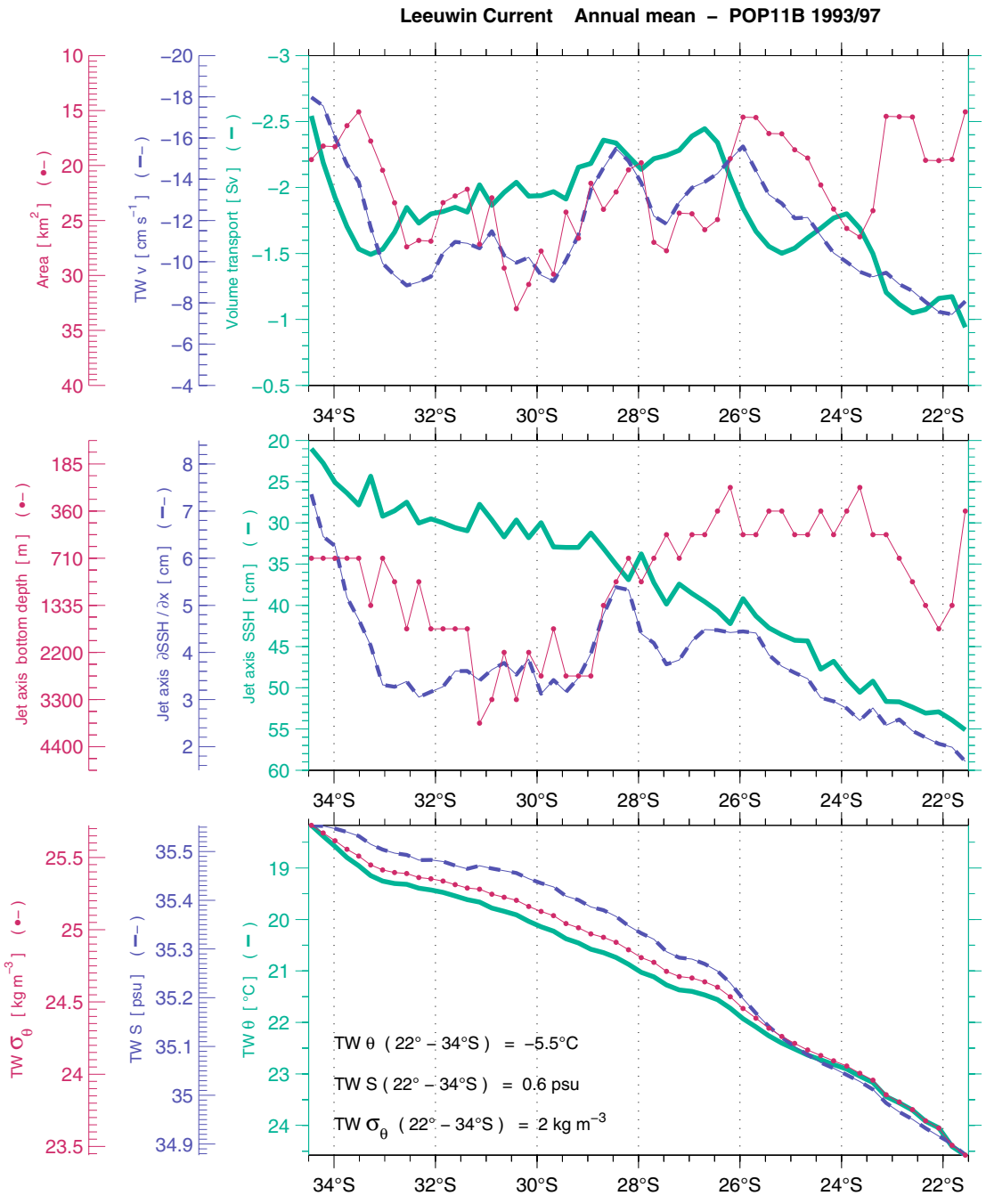

Figure 5.3. Mean volume transport, transport–weighted velocity and area (top panel). SSH, cross–shore SSH gradient, bottom depth along the Leeuwin Current axis (middle panel). Transport–weighted θ, salinity and σ_θ (bottom panel). From 22°S to 34°S, the Leeuwin Current became cooler (–5.5°C), saltier (0.6 psu) and denser (2 kg m^{-3}).

5.4 SEASONAL CYCLE

5.4.1 Current structure and property distributions

The seasonal cycle of the Leeuwin Current is illustrated by the model slice taken at its core depth at 37.5 m depth in **Figures 5.4**, **5.5**, and **5.6**. From December to March the current is quiescent but it suddenly pulses in April and evolves into a vigorous poleward flow during wintertime. Instabilities are set off and begin to grow after the current becomes highly energetic in May. The vigorous Leeuwin Current dissipates a large amount of its energy between June and August, by actively shedding mesoscale eddies into the adjacent southeast Indian Ocean. Even though the monthly mean panels are a 5–year average (1993/97), the wintertime eddy variability remains conspicuous. The generation of the mesoscale eddies are not only a form of dissipation of momentum/ energy but also a way to exchange water properties and other tracers between the boundary and the ocean interior. From September to November, the energy levels of the Leeuwin Current gradually decay and it returns to its summertime condition.

SSH anomalies [**Figure 5.7**] reveal that the "April pulse", associated with the poleward acceleration of the Leeuwin Current appears triggered by the anticlockwise propagation of a coastally trapped Kelvin wave that quickly transmits a positive sea level anomaly around the northwestern, western and southwestern coasts of Australia [Godfrey and Golding, 1981; Godfrey and Weaver, 1991]. The current instabilities emerging after the passage of this wave are mostly recognised by positive sea level anomalies growing at the boundary (May and June), detaching from the Leeuwin Current (July to September), and subsequently moving to the offshore deep ocean, where they tend to decay. They may be interpreted as eddies propagating at Rossby wave speeds (or westward propagating Rossby waves) excited by the Kelvin wave travelling along the Australian coast [Potemra, 2001]. Instabilities of the Leeuwin Current have been reported to be of mixed barotropic and baroclinic type because of strong lateral and vertical shears [Batteen *et al.*, 1992; Batteen and Butler, 1998; Feng *et al.*, 2005b].

The poleward acceleration of the Leeuwin Current in April prompts the faster advection of warmer and fresher Tropical Water to the west Australian coast, from a coastally trapped area on the southern part of the North West Shelf (warmest/freshest) and from the offshore ocean through veering of eastward jets near the coastal boundary. The warmest and freshest water seems to be advected inshore of the current axis north of 30°S [see also mean in **Figure 5.1**]. The offshore surface salinity maximum is more salient during April and May (>35.7 psu) and tends to be fresher from July to December.

The vertical structure of the seasonal Leeuwin Current is shown in **Figures 5.8** (January), **5.9** (April), **5.10** (July) and **5.11** (October). These figures were based on the mask which identified the mean position of the Leeuwin Current. Although the Leeuwin

Current meanders seasonally, a lot of effort would be required to unmistakably identify what is only Leeuwin Current and create monthly masks using a streamwise approach. From what we have verified, the "mean position" mask is not ideal but does a reasonable job in picking up the seasonal Leeuwin Current. One aspect in the sections that instantly stands out is the poleward reversal of the mean equatorward flow of the undercurrent during the passage of the "April pulse" that spins up the Leeuwin Current. In addition to this, the vertical sections provide insight into other water column variations. In January the top 50 m is highly stratified, more intensely in the tropics, yet strongest in April. The stratification weakens towards winter and gives rise to deep mixed layers. Water properties of the Leeuwin Current are vertically homogeneous in July, most possibly as a result of winter convection. Restratification sets in during springtime when a seasonal thermocline is reformed (October). For instance, the subsurface salinity minimum seen in January and April disappears in July but resurfaces once more in October.

Shallow upwelling prevails in January when the climatological equatorward large scale wind stress is at its maximum and favours offshore Ekman transport. The April pulse causes a coherent downwelling over most of the domain, from near surface down to 800 m depth, consistent with downward energy propagation (upward phase propagation). The pattern of the vertical velocity field comprising elongated downward cells interposed in a few upward cells during the intense mesoscale activity period in winter (July) as well as during its decay period in spring (October) seems to arise from vertical excursions of the thermocline caused by that activity which is not perfectly averaged out over 5 years. The mesoscale eddies tend to have a deep reach, at least down to 800 m, and so not simply confined to Leeuwin Current depths.

5.4.2 Volume transport and transport–weighted properties

Although the Leeuwin Current spins up in April, the bulk of its poleward transport occurs during May–June, with peaks as large as –4.0 to –4.5 Sv (26°S and 32°S) [**Figure 5.12**]. This is also the time when the equatorward wind stress is weakest (not shown). No reversal of the current is seen. The smaller scale noise in the diagram mostly originates from the seasonal meandering of the Leeuwin Current outside the limits of its "mean position" mask. As a result, some of its transport has not been captured, such as over 22°–26°S in April, May and June, and at 30°S in June [**Figure 5.4**]. Despite the current being fully captured near Cape Leeuwin (34°S), its transport pattern is distinct from the other latitude bands. In this region, the Leeuwin Current starts to spin up in April but just reaches its peak during July–August and then remains relatively strong until November–December. This modified seasonality appears to be related with variations in a narrow near surface eastward jet that veers into the Leeuwin Current nearby 34°S [**Figure 5.4**]. Because the transport peak is long lived, it results in a larger mean [**Figure 5.3**, top panel]. Godfrey *et al*. [1986] and Cresswell and Peterson [1993] have earlier reported dynamical changes in the Leeuwin Current when it approaches Cape Leeuwin.

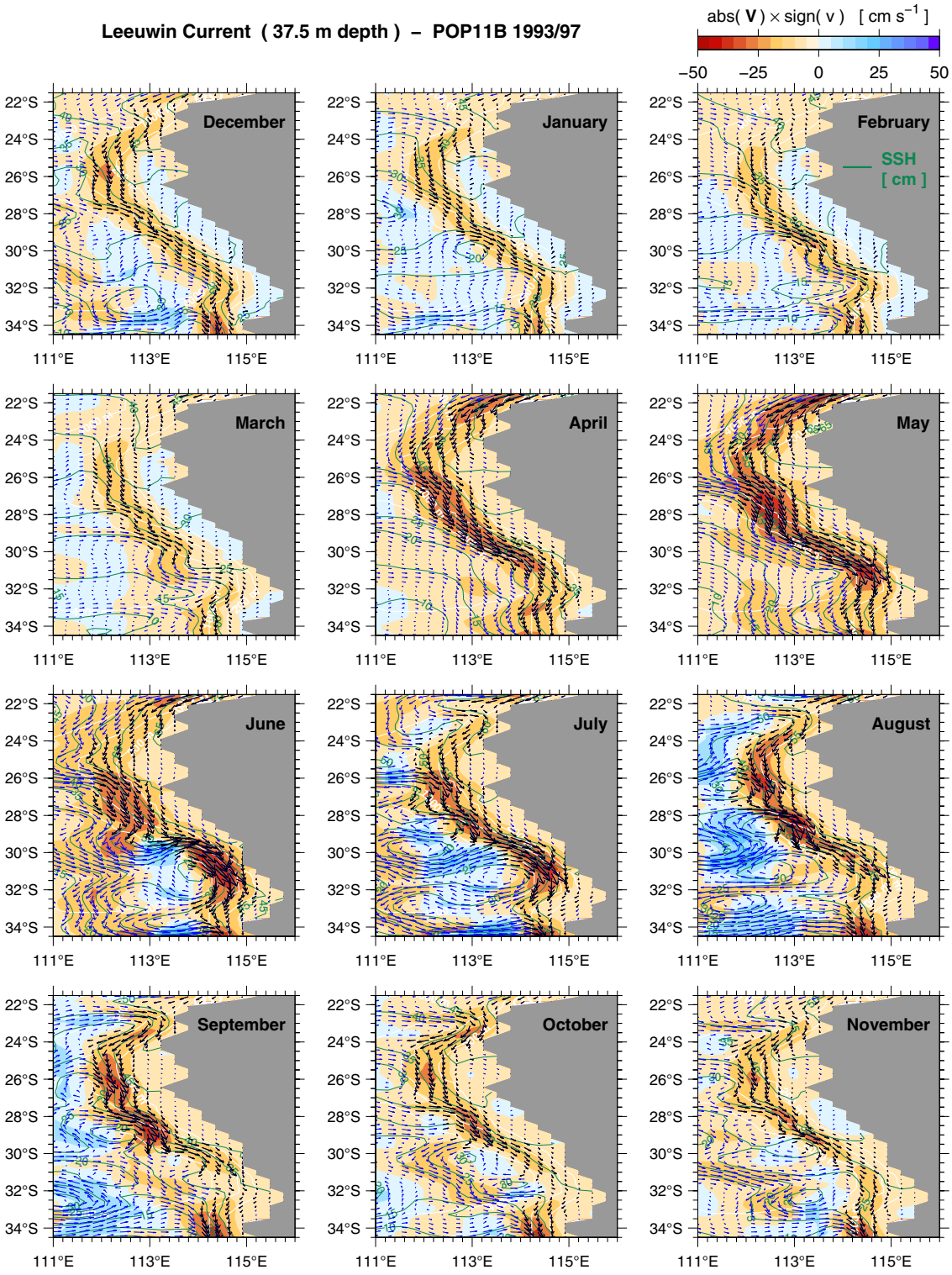

Figure 5.4. Seasonal velocity vectors at 37.5 m. Velocity vectors are superimposed on the absolute speed (**V**) multiplied by the sign of the meridional velocity (+N). SSH contours are indicated in green and isobaths in white. Vectors in black are part of the "mask" (see text).

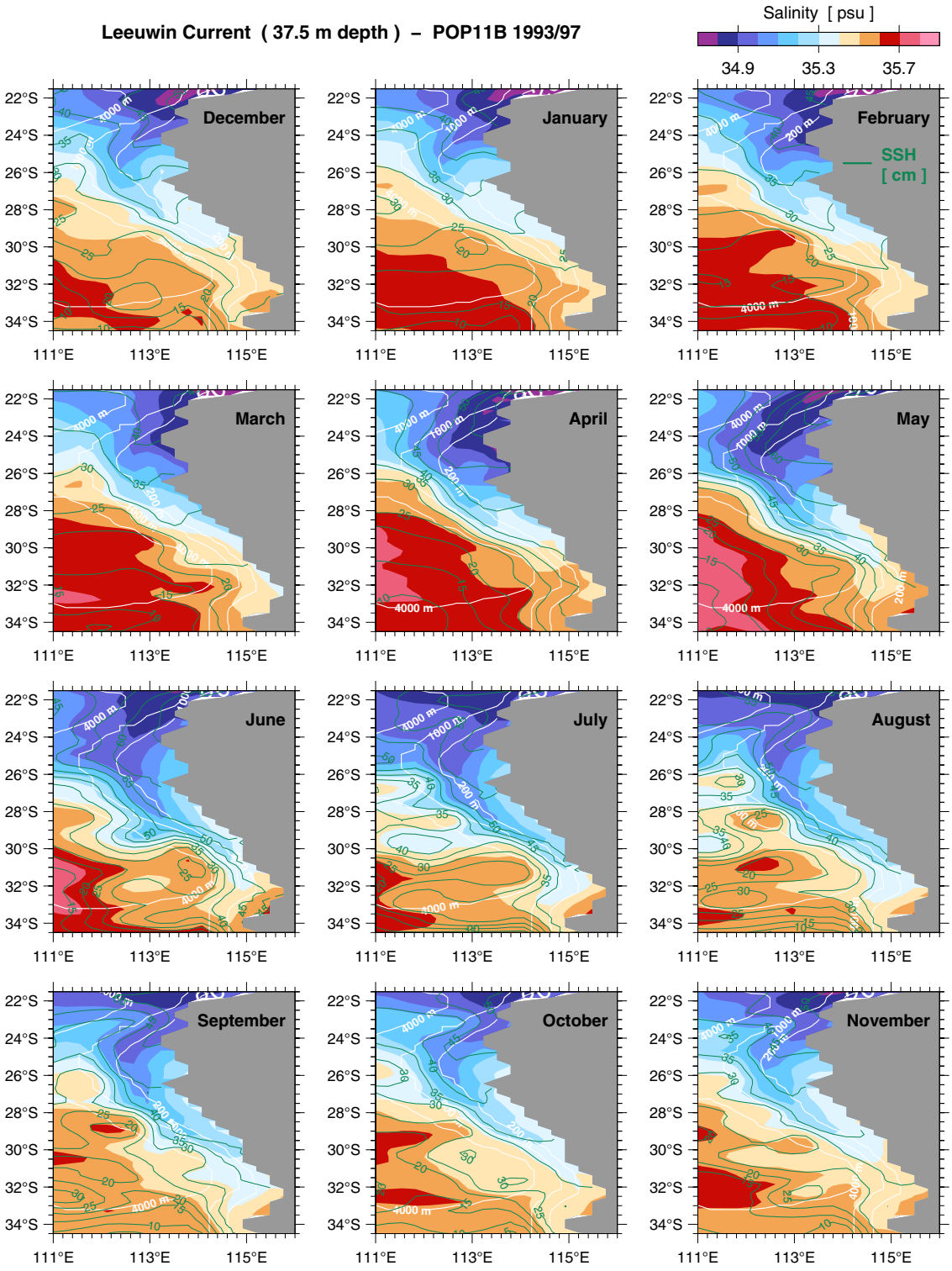

Figure 5.5. Seasonal salinity at 37.5 m depth. SSH contours are indicated in green and isobaths in white.

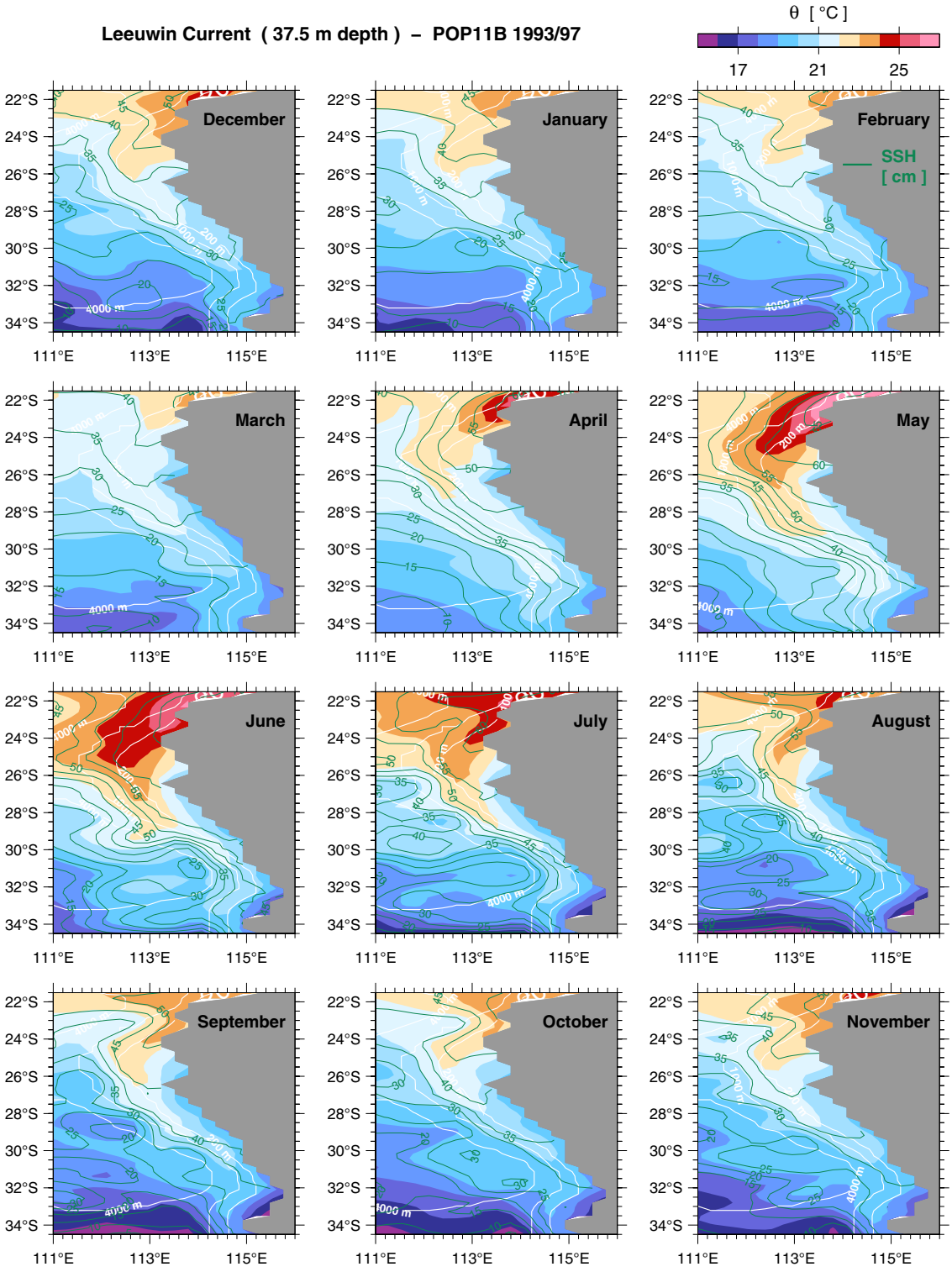

Figure 5.6. Seasonal θ at 37.5 m depth. SSH contours are indicated in green and isobaths in white.

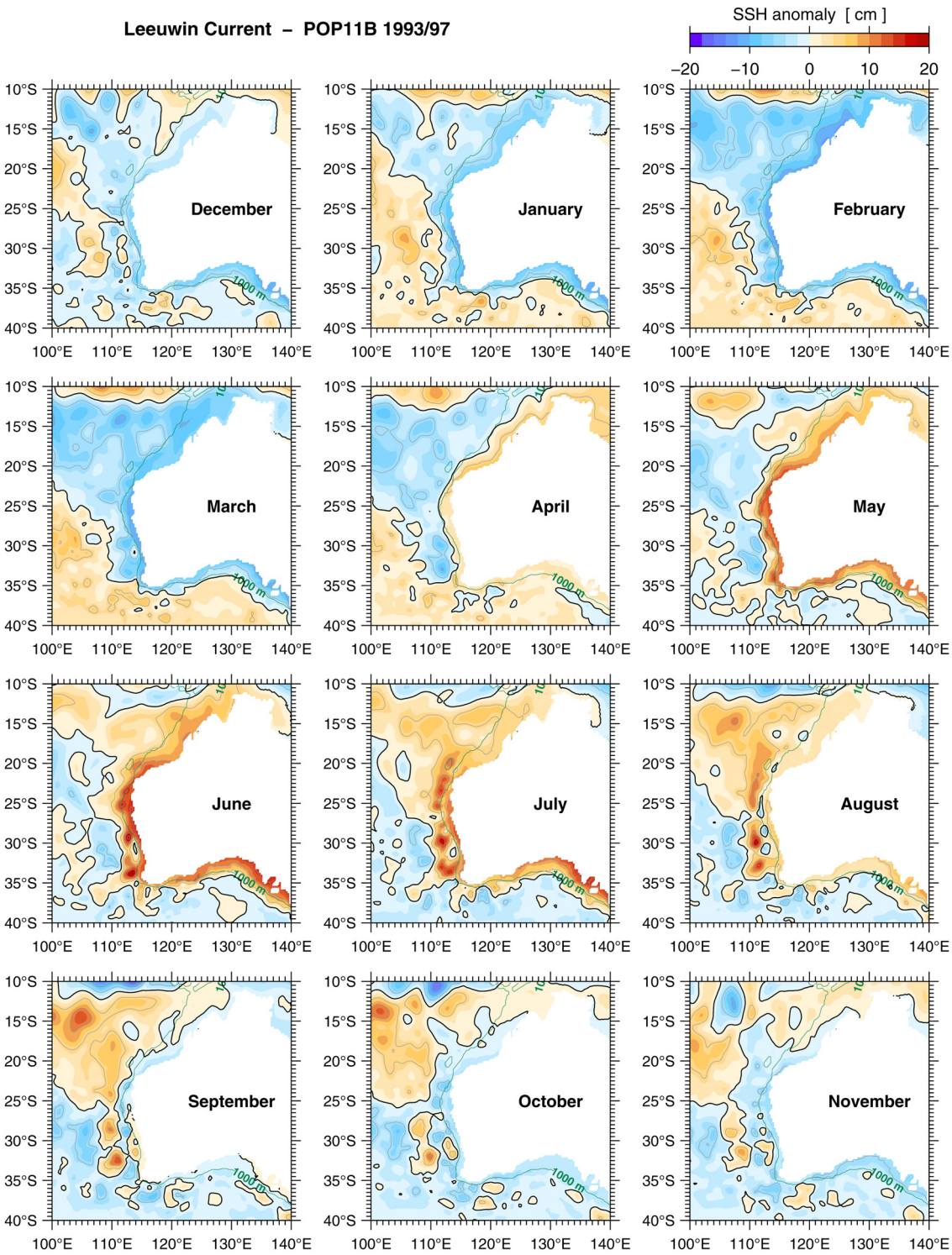

Figure 5.7. Seasonal SSH anomaly (zero line in bold black). The 1000 m isobath is the green line.

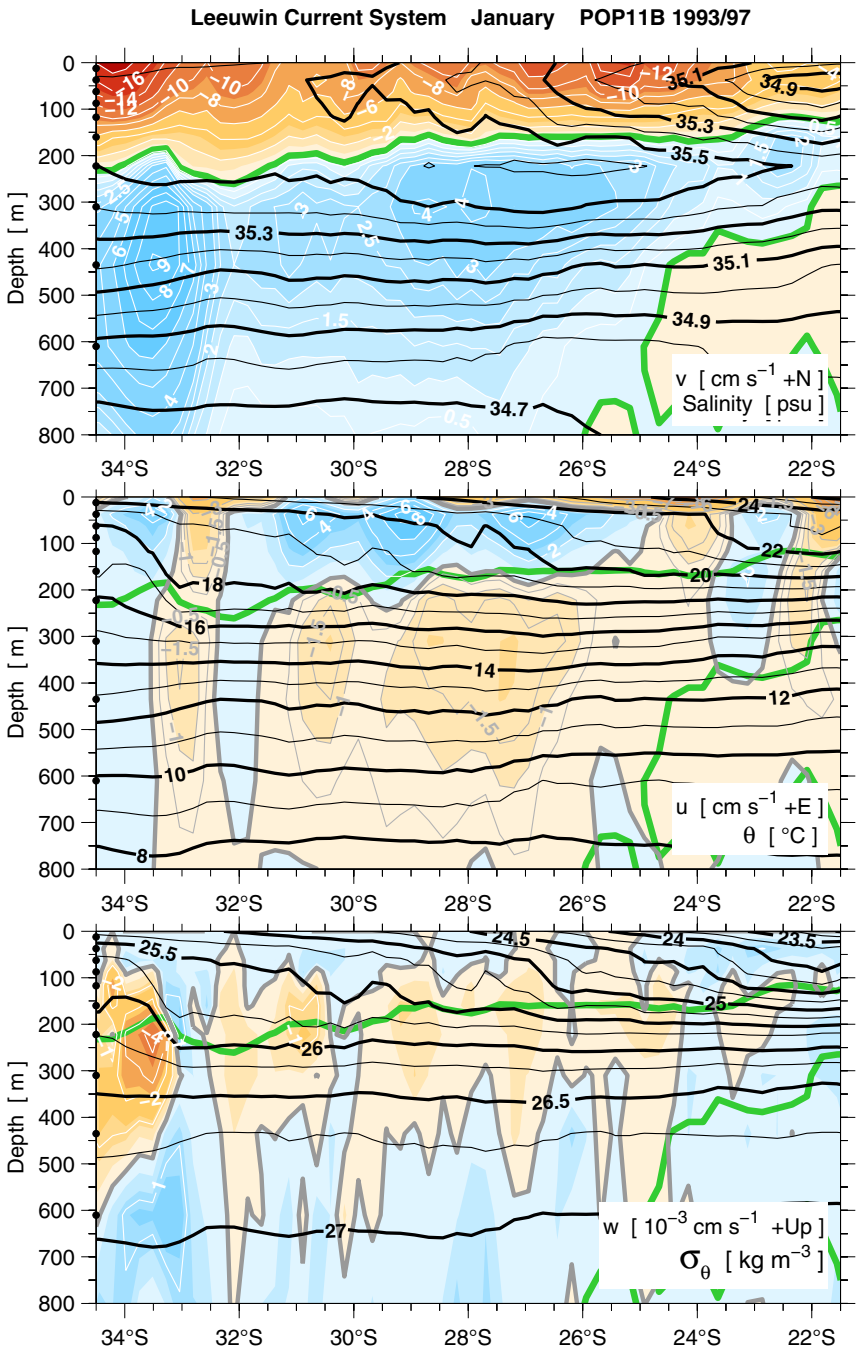

Figure 5.8. January vertical section. Salinity and meridional velocity (top). θ and zonal velocity (middle). σ_θ and vertical velocity (bottom). The bold green contour is the meridional velocity zero line on all plates.

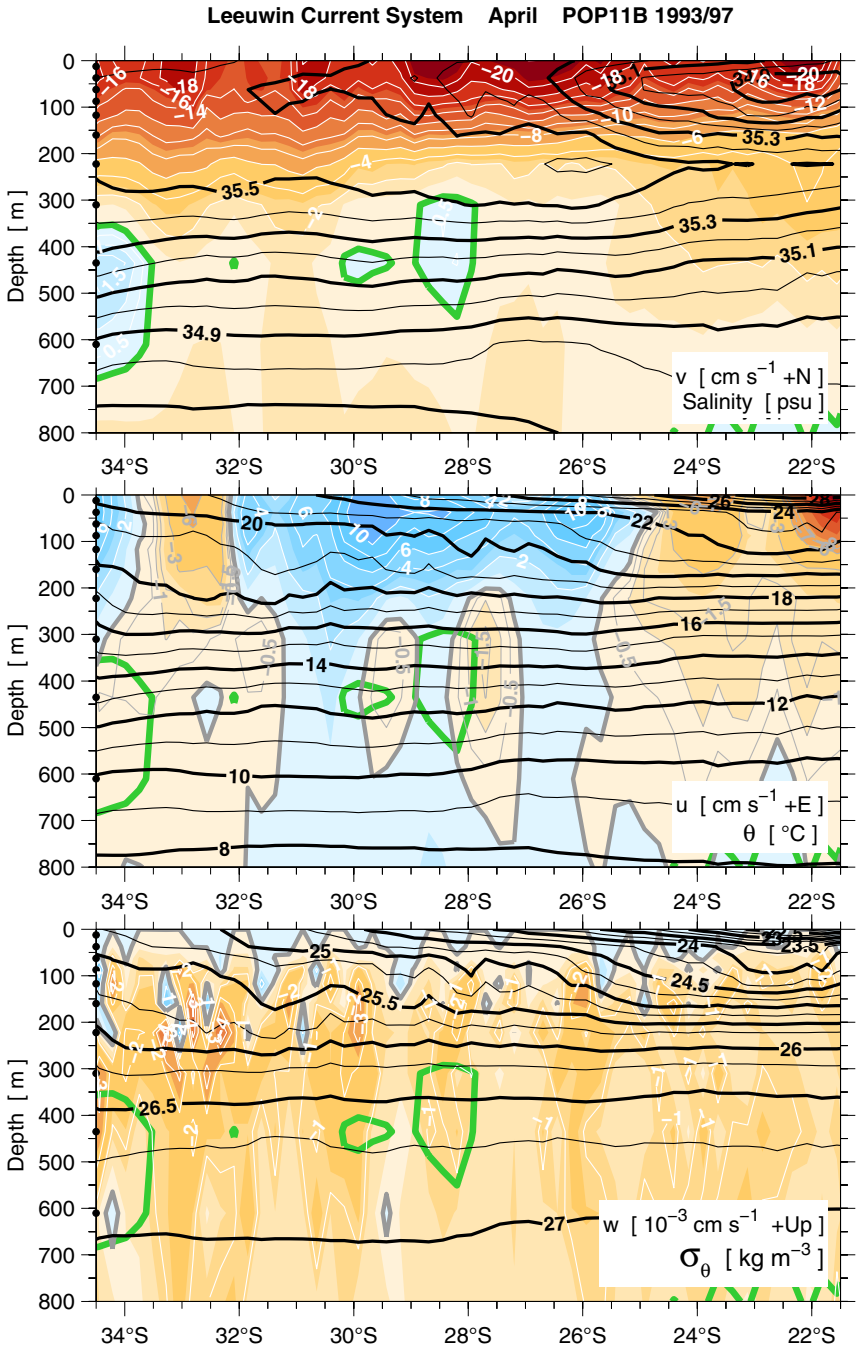

Figure 5.9. April vertical section. Salinity and meridional velocity (top). θ and zonal velocity (middle). σ_θ and vertical velocity (bottom). The bold green contour is the meridional velocity zero line on all plates.

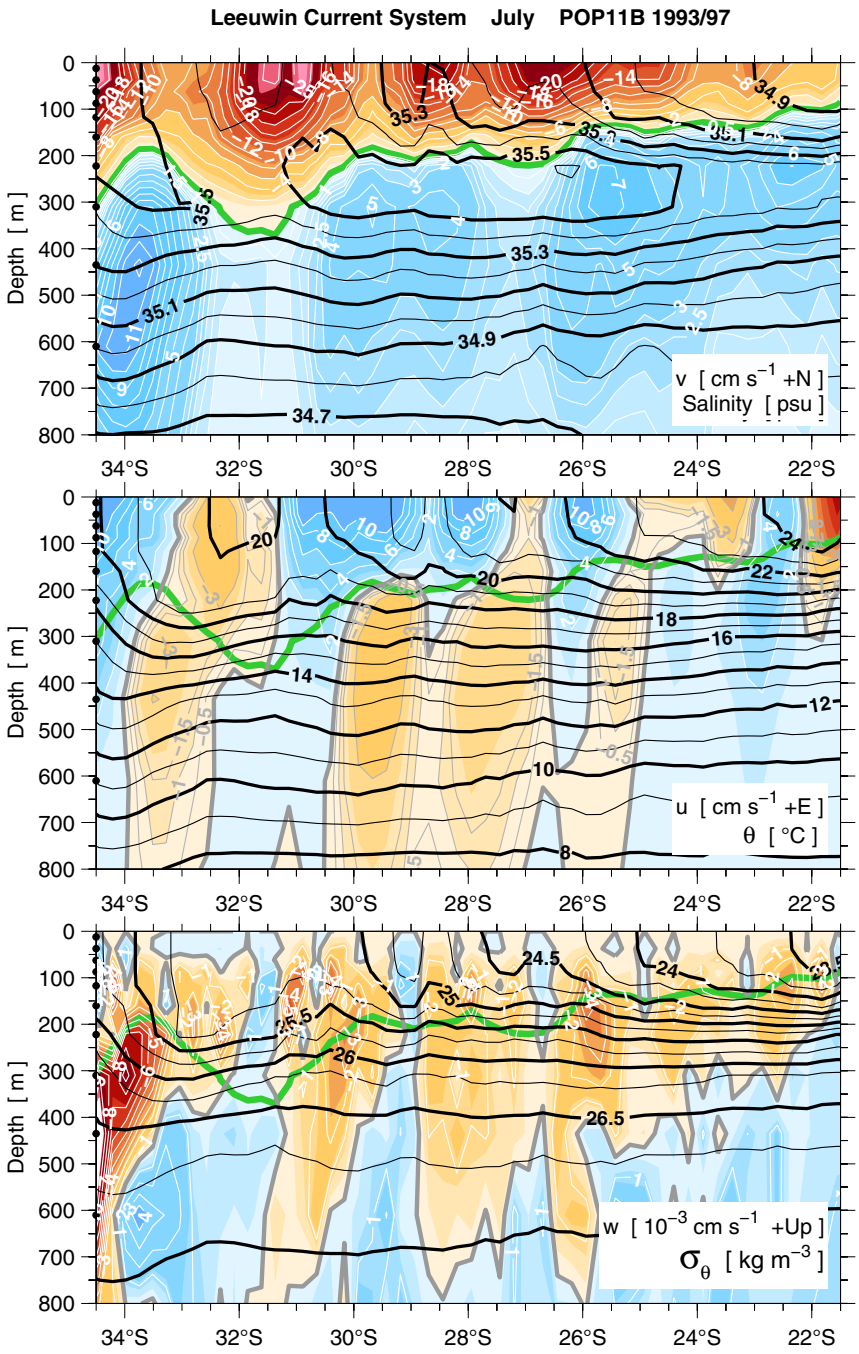

Figure 5.10. July vertical section. Salinity and meridional velocity (top). θ and zonal velocity (middle). σ_θ and vertical velocity (bottom). The bold green contour is the meridional velocity zero line on all plates.

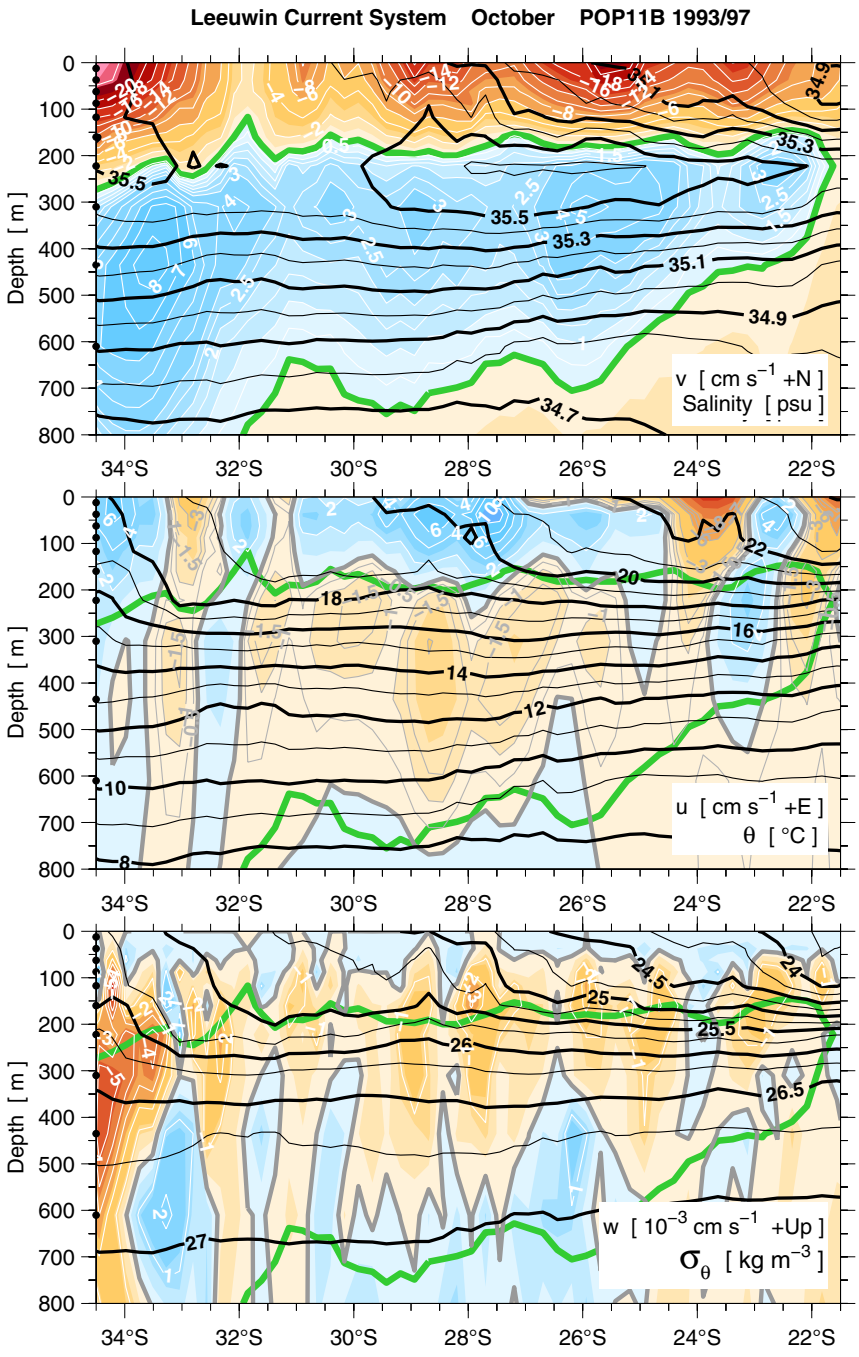

Figure 5.11. October vertical section. Salinity and meridional velocity (top). θ and zonal velocity (middle). σ_θ and vertical velocity (bottom). The bold green contour is the meridional velocity zero line on all plates.

The transport–weighted salinity [top panel] and θ [bottom panel] diagrams in **Figure 5.13** depict the progression of the fresh and warm tongue during autumn and winter along the west Australian coast, favoured by a stronger downstream advection triggered by the April pulse (SSH contours) and a simultaneously weaker equatorward wind stress (not shown). The advection of this rather light water creates a maximum in SSH along the entire coast during April–May–June. If an average is taken, from 22°S to 34°S [**Figure 5.14**], the Leeuwin Current is freshest in July (most saline in March) [top right], warmest in May (coldest in September) [bottom right], and lightest in June (densest in September) [bottom right]. The volume transport is maximum in May [top left] while the SSH is highest in June [bottom left]. The subtle secondary peak in SSH during November seems to represent the quasi–semi annual (Rossby wave) signal first documented in Morrow and Birol [1998], however, this variability either does not carry any signature in the water properties or its is obscured by other processes.

5.5 HOW REALISTIC ARE THE MODEL RESULTS ?

The water properties of the model are to some extent different from the real ocean. In general, Tropical Water is warmer and saltier whereas Subtropical Water is fresher and cooler. For instance, the model cannot reproduce the ≥35.8 psu within the Leeuwin Undercurrent at 22°S as observed in the ICM6 data [see **Chapter 3**]. The mean volume transport of the Leeuwin Current is –1.8 Sv at 32°S compared to the –3.2 Sv in Feng *et al*. [2003]. This smaller model value is expected as POP11B is only eddy–permitting and cannot resolve the entire spectrum of the energy levels involved in the ocean dynamics. As the model mixed layer formulation performs poorly, this perhaps causes a too strong Ekman transport in the top 25 m, and consequently the shallow upwelling in the upper portion of the Leeuwin Current might be somewhat exaggerated. The seasonal variability of the Leeuwin Current in the θ–S plane (not shown) shows a large jump in water properties between the top and remaining depth layers during seasons other than winter, when the Leeuwin Current is more stratified. This seems to result from the poor parameterisation of the vertical mixing scheme in midlatitudes, as it was originally developed for the tropics. The situation is also worsened by the fact that vertical mixing is solved explicitly, which means that sometimes the vertical diffusion coefficients have to be lowered for numerical stability and consequently water properties are not sufficiently mixed in the vertical [Griffies and Maltrud, *pers. comm.*]

Despite the limitations reported above, the mean and the seasonal variability of the Leeuwin Current in the model, both in terms of transport and water properties, are in quite good agreement with field and remote observations, and simulates much of what has been known. Various snapshots of the Leeuwin Current have suggested that the current tapers, deepens and accelerates as it moves downstream along the west

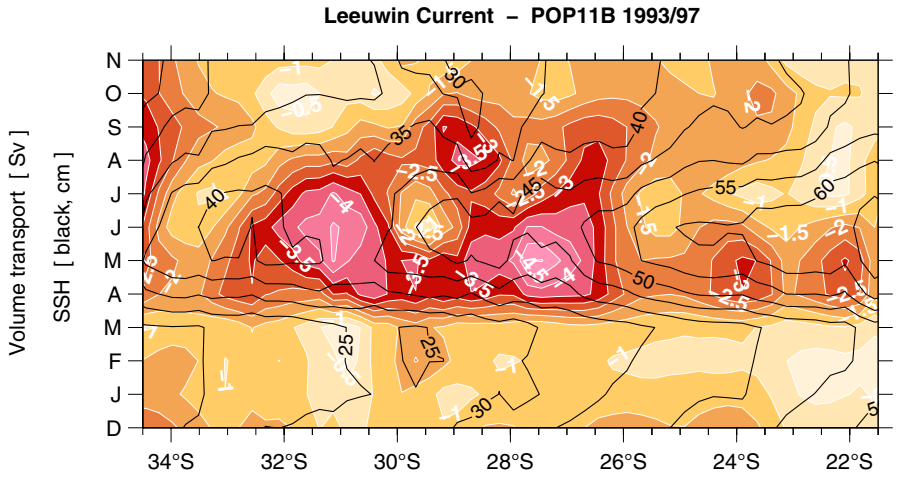

Figure 5.12. Seasonal volume transport of the Leeuwin Current jet off Western Australia. SSH is contoured in black.

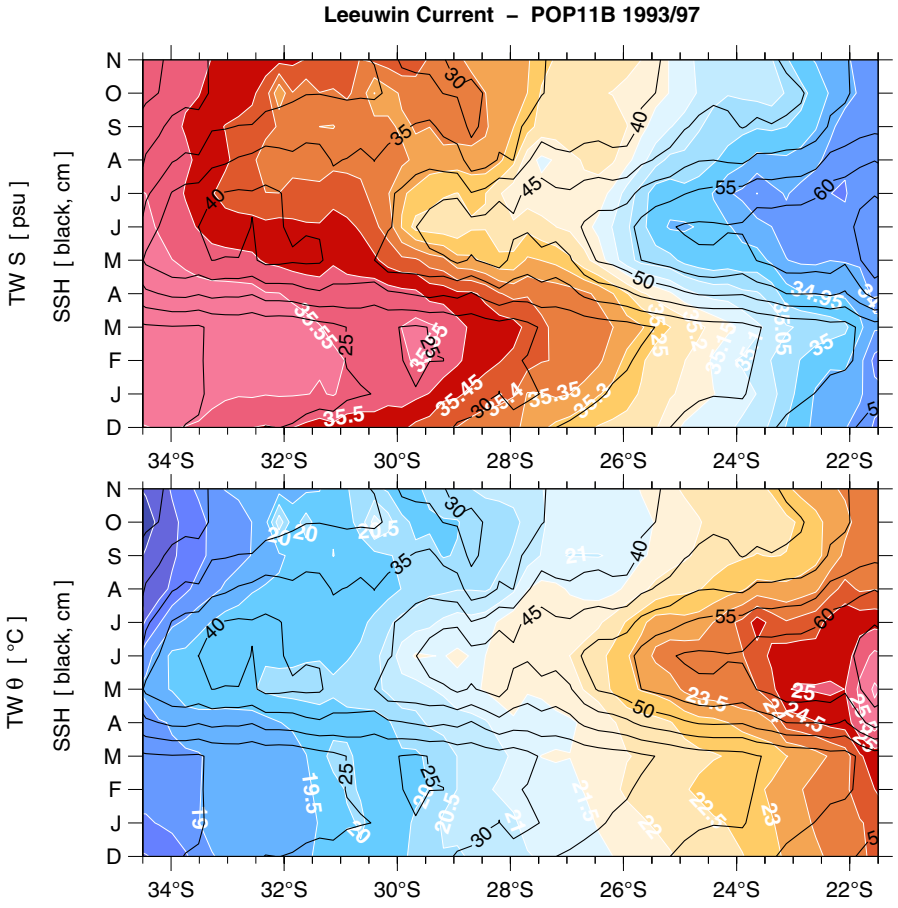

Figure 5.13. Seasonal transport–weighted salinity (top) and θ (bottom) of the Leeuwin Current jet off Western Australia. SSH is contoured in black.

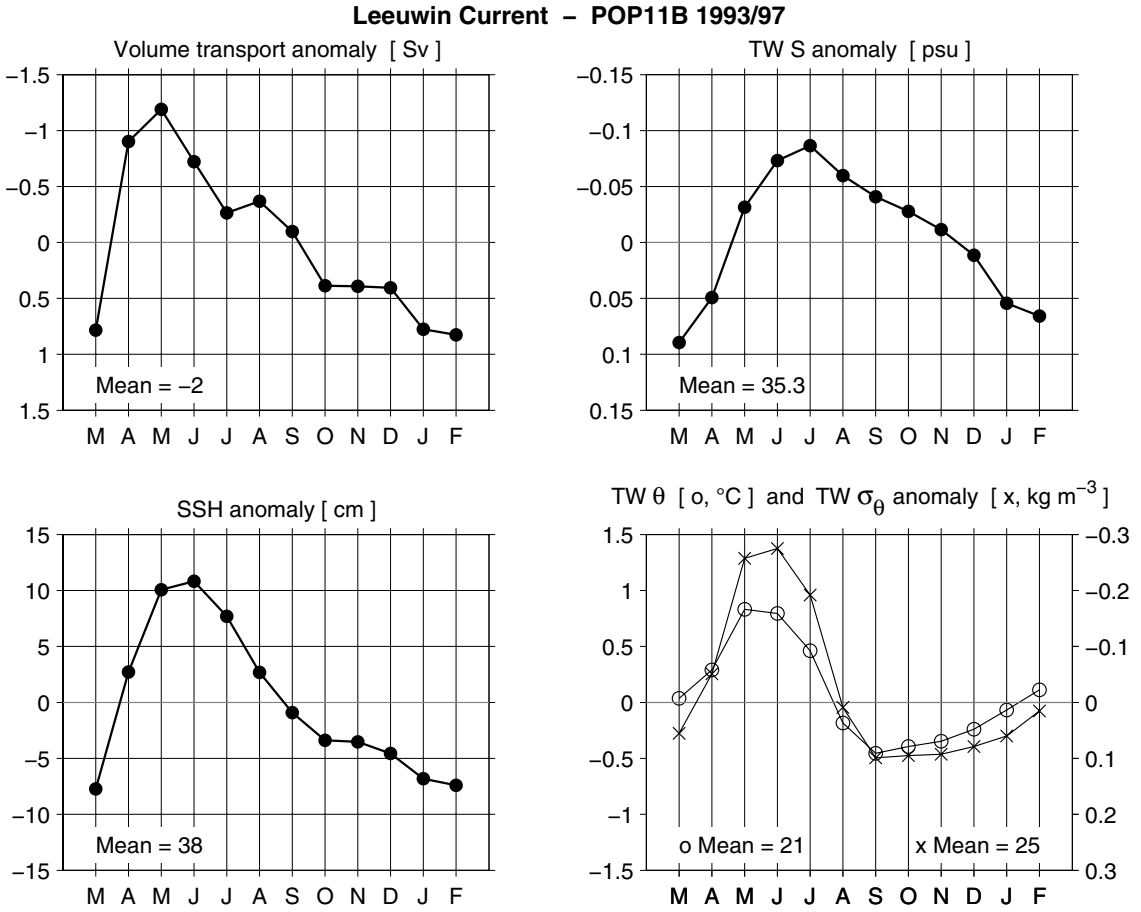

Figure 5.14. Seasonal anomalies of the Leeuwin Current jet averaged over 22°–34°S. Volume transport (top left). Transport–weighted salinity (top right). SSH (bottom left). Transport–weighted θ (left axis) and σ_θ (right axis) (bottom right).

Australian coast [e.g., Church *et al.*, 1989]. Although we do verify a tapering of warm and fresh water near 22°S, we have only defined the Leeuwin Current based on its boundary current flow. The current does uniformly deepen towards higher latitudes, from about 150 to 300 m depth, as previously suggested in the above literature review. It also accelerates downstream and is strongest and fastest near 34°S, however, the acceleration is not uniform and there are sites where it actually decelerates. The stronger poleward advection of warm fresh Tropical Water down Western Australia in April, implied by thermal observations of Gentilli *et al.* [1972] has been quantified in the model. The ~6°C cooling of the Leeuwin Current along its poleward path is very close to the estimate obtained by Ridgway and Condie [2004] using sea surface temperature from satellite measurements. The model sea surface height anomaly associated with the annual Kelvin wave is likewise described in altimetric observations [Ridgway and Condie,

2004]. Potemra [2001] implies that a westward propagating annual Rossby wave, forced by the wind stress in the western tropical Pacific, impinges on the Indonesian archipelago and allows the leaking of a Kelvin wave that travels along the Australian coast, similarly to the well documented Rossby–Kelvin wave mechanism at an interannual scale [e.g., Clarke and Liu, 1994; Wijffels and Meyers, 2004]. The passage of the Kelvin wave, in turn, besides intensifying the Leeuwin Current, excites instabilities that radiate westward propagating Rossby waves [Potemra, 2001]. Even a quasi semi–annual signal first reported in Morrow and Birol [1998] is detected in the model. The map of mean SSH from POP11B agrees quite well with the mean surface steric height distribution, based on the CARS atlas [Ridgway *et al.*, 2002], shown in Ridgway and Condie [2004]. Both fields imply on the existence of a number of narrow subtropical eastward jets off Western Australia.

So, in sum, despite some discrepancies, we are confident that the POP11B model is satisfactorily reproducing the kinematics of the upper southeast Indian Ocean under investigation in this study. The quantitative estimates are not quite like the real ocean, however, they are a good guide for the order of the magnitude of the processes.

5.6 CONCLUSIONS

On the mean, the Leeuwin Current is a poleward flow found year–round along the west Australian coast, between 22°S and 34°S. It progressively deepens, from 150 m to 300 m, but does not uniformly accelerate downstream. There are three distinct regions in which the poleward transport increases or decreases following net lateral inflows or outflows along its outer edge [**Figure 5.15**]. It basically starts with –1.2 Sv at 22°S; gains another –1.1 Sv between 22°–27°S through a net eastward inflow; loses –0.8 Sv through a net westward outflow between 27°–33°S; and finally gains –0.7 Sv through a second net eastward inflow, increasing its transport to –2.2 Sv at 34°S. In terms of transport–weighted salinity, θ and σ_θ the Leeuwin Current respectively gains 0.6 psu, loses 6°C and gains 2 kg m^{-3} along its path from North West Cape (22°S) to Cape Leeuwin (34°S). Part of these changes must be due to air–sea fluxes and part due to lateral exchanges with the adjacent ocean.

The seasonal variation of the Leeuwin Current appears primarily driven by the anticlockwise progression of an annual Kelvin wave, evident as a coastal positive sea level anomaly in April off Western Australia [Godfrey and Ridgway, 1985; Ridgway and Condie, 2004; Potemra, 2001]. The Leeuwin is in a quiescent state in summertime (–0.5 to –1.5 Sv) but by April the wave pulse propagates down the west Australian coast and triggers a strong poleward advection of warm and fresh water from the tropics (north of 22°S). This poleward flow arises from the geostrophic adjustment to the large cross–shore SSH gradient created by the wave. During May–June the Leeuwin Current achieves its transport peak (–4.0 to –4.5 Sv) and is freshest and warmest. Soon after it becomes

vigorous, instabilities grow and evolve into wavelike meanders and mesoscale eddies, which detach from the boundary and migrate offshore. July–August is the period when the eddy activity is most intense. From September, the activity begins to decay and the Leeuwin Current progressively returns to its summertime condition. A departure from this seasonal variation appears near Cape Leeuwin (34°S), where the transport maximum lasts from April to November apparently due to variations in an eastward subtropical jet that feeds into the boundary flow of the Leeuwin Current [**Figure 5.4**]. This gives rise to an abrupt increase in the estimates over a short distance as seen in the mean, south of 33°S [**Figure 5.3**, top panel].

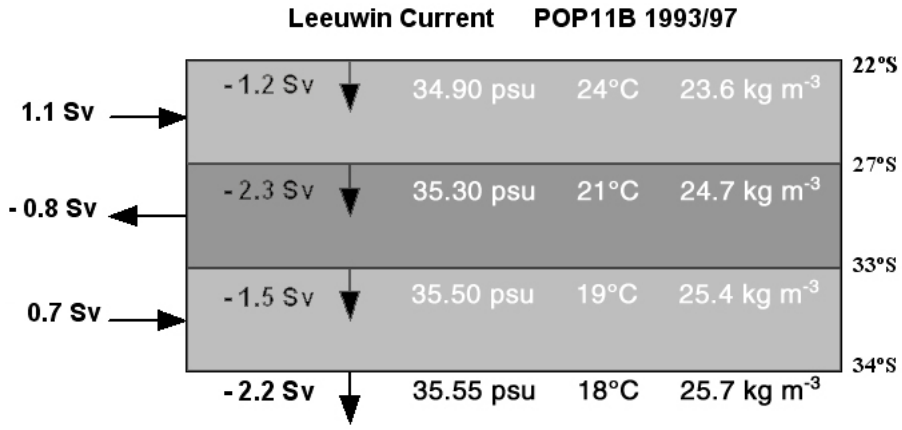

Figure 5.15. Schematic of the mean Leeuwin Current jet transport and its transport–weighted properties from 22°S to 34°S.

The mean and seasonal description of the Leeuwin Current in this study does not give much insight on the relationship of its poleward boundary flow with the eastward subtropical jets that are known to feed into it [see **Chapter 4**]. The reasons are twofold. First, the Tropical Water transported downstream from the tropics is modified by air–sea fluxes and becomes saltier and cooler, more like Subtropical Water. Second, there seems to be a substantial amount of lateral exchange between the poleward jet and the adjacent ocean, so it is quite hard to set apart the Subtropical Water contribution that comes from offshore. In addition, although eastward flows can be pinpointed in the current fields, their pathways into the boundary involve a complicated three dimensional motion, as detected in **Chapter 4**. They can either feed into the Leeuwin Current or the Leeuwin Undercurrent. The most appropriate way to address the impact of these subtropical jets is to carry out a quantitative Lagrangian analysis. From the mean depth structure of the Leeuwin Current presented in this study, however, one deep salinity maximum is clearly recognised as Subtropical Water (>35.5 psu) transported by eastward jets into the boundary between 26°–32°S.

Much of what has been learnt about the Leeuwin Current in the past has been based on a large amount of assembled qualitative field information and on a few long term direct observations (but these no longer than 1–2 years). Feng *et al.* [2003] were the first to provide a solid quantitative picture of the mean, annual and interannual variability of the Leeuwin Current which was based on a high resolution historical upper ocean climatology. However, this picture is from one specific coastal site at 32°S. In this study, we provide a more comprehensive picture of the mean and seasonal Leeuwin Current over the entire coast of Western Australia, from 22°S to 34°S, using the 5–year long POP11B 1993/97 model outputs. The results confirm a number of features suggested in past observational studies, bring some more details and a few new insights. They also quantify the water properties and current structure of the Leeuwin Current in the large scale context of the adjacent southeast Indian Ocean. This will work as a benchmark for future studies on the system.

The changes in properties of the Leeuwin Current quantified in this chapter are governed by air–sea fluxes and also by water exchange with the adjacent ocean interior. In the next chapter, we examine the relative contribution of these two mechanisms in the cooling of the Leeuwin Current, from North West Cape (22°S) to Cape Leeuwin (34°S).